MDPI

Article

Noise Transfer Approach to GKP Quantum Circuits

Timothy C. Ralph [1,*] , Matthew S. Winnel [1] , S. Nibedita Swain [1,2,3] and Ryan J. Marshman [1]

[1] Centre for Quantum Computation and Communication Technology, School of Mathematics and Physics, University of Queensland, Brisbane, QLD 4072, Australia; mattwinnel@gmail.com (M.S.W.); nibedita.iiser@gmail.com (S.N.S.); r.marshman@uq.edu.au (R.J.M.)
[2] School of Mathematical and Physical Sciences, University of Technology Sydney, Ultimo, NSW 2007, Australia
[3] Sydney Quantum Academy, Sydney, NSW 2000, Australia
* Correspondence: ralph@physics.uq.edu.au

Abstract: The choice between the Schrödinger and Heisenberg pictures can significantly impact the computational resources needed to solve a problem, even though they are equivalent formulations of quantum mechanics. Here, we present a method for analysing Bosonic quantum circuits based on the Heisenberg picture which allows, under certain conditions, a useful factoring of the evolution into signal and noise contributions, similar way to what can be achieved with classical communication systems. We provide examples which suggest that this approach may be particularly useful in analysing quantum computing systems based on the Gottesman–Kitaev–Preskill (GKP) qubits.

Keywords: quantum computing; cat states Bosonic codes

1. Introduction

A useful technique for analysing quantum optical experiments based on Gaussian operations and measurements is the quantum noise transfer approach [1], which is characterised by a displacement vector and a covariance matrix [2]. Working in the Heisenberg picture, the signals (the displacements) and the quantum noise (the covariances) can be tracked separately, in much the same way that signals and noise are tracked, for example, in classical communication systems. A key step in such an analysis is the definition of quadrature fluctuation operators:

$$\delta\hat{q} = \hat{q} - q, \quad \delta\hat{p} = \hat{p} - p, \tag{1}$$

where $q = \langle\hat{q}\rangle$ and $p = \langle\hat{p}\rangle$ are real numbers representing the average values of the position and momentum quadrature displacements, respectively. Also, $\hat{q}$ and $\hat{p}$ are the position and momentum operators for the mode in question, respectively. We use the convention that the annihilation operator for the mode is given by $\hat{a} = 1/2(\hat{q} + i\hat{p})$, which can then be expanded as follows:

$$\hat{a} = 1/2(q + \delta\hat{q} + i(p + \delta\hat{p})), \tag{2}$$

and the classical signals (displacements) and the quantum noise operators can be independently tracked in the Heisenberg picture through various interactions and measurements in an intuitive way. In an experimental setting, the noise properties of the input states can be measured directly by subtracting the known signal and evaluating the variance of the quantum fluctuations. For example, the position quadrature variance is

$$V_q \equiv \langle\delta\hat{q}^2\rangle = \langle(\hat{q} - q)^2\rangle = \langle\hat{q}^2\rangle - q^2 \tag{3}$$

The aim of this paper is to develop an analogous approach which can describe the evolution of non-Gaussian states, such as cat states [3] or Gottesman–Kitaev–Preskill (GKP) states [4], in a similar way. Such states are formed from a superposition of differently displaced states, and hence the signal is multi-valued.

In the next section, we will introduce our new decomposition into signal and fluctuation operators and show how noise properties can be analysed independent of the signal value, provided certain conditions are met. We illustrate this with cat state and GKP state examples. In Section 3, we consider the Heisenberg picture evolution of our operators, with loss and feedforward as examples. In Section 4, we apply our formalism to GKP states and analyse a teleportation channel which includes the GKP error correction protocol. The goal is to evaluate the noise transfer properties of the circuits based on the first and second moments of the resource states (and the properties of the feedforward measurements), thus providing an alternative method for analysing quantum computing circuits based on GKP qubits. Current approaches to GKP circuit evaluation are based on Schrödinger picture analysis. Noise can be added to ideal GKP states [5], and the logical states can be tracked through a modular sub-system decomposition [6], which can be generalised to finite-energy GKP states [7,8]. Exact numerical models incorporating noisy elements have also been explored [9]. In contrast, the method presented here differs by describing a way to empirically quantify the noise and signals independently and then track them through circuits via their Heisenberg evolution, offering potential advantages in the intuitive nature of the approach and the tractability of the calculations in the presence of multiple noise sources. We discuss our results and conclude this work in Section 5.

2. Signal and Fluctuation Operators

We start by defining the operators $\delta\hat{q}$ and $\delta\hat{p}$ in a way analogous to Equation (1) as follows:

$$\delta\hat{q} = \hat{q} - \hat{q}_c, \quad \delta\hat{p} = \hat{p} - \hat{p}_c. \tag{4}$$

Because the displacements are multi-valued, they must be represented by operators, specifically $\hat{q}_c$ and $\hat{p}_c$. We characterise $\hat{q}_c$ and $\hat{p}_c$ by their moments over restricted domains around their expected displacement values in the position and momentum quadratures, respectively. Specifically, given that $q_n = \langle\hat{q}\rangle_n$ is the expectation value for q values falling in the nth position domain, we require that $\langle\hat{q}_c\rangle_n = q_n$. We further require that $\langle\hat{q}_c^2\rangle_n = q_n^2$, meaning that $\hat{q}_c$ has zero variance in each domain. This implies that $\langle\hat{q}\hat{q}_c\rangle_n = q_n^2$. Similarly, we require $\langle\hat{p}_c\rangle_n = p_n$, where $p_n = \langle\hat{p}\rangle_n$ is the expectation value for p values falling in the nth momentum domain, $\langle\hat{p}_c^2\rangle_n = p_n^2$, and hence $\langle\hat{p}\hat{p}_c\rangle_n = p_n^2$. Assuming that we have N_q position domains and N_p momentum domains, the full expectation values are given by

$$\langle\hat{q}_c\rangle = \sum_n^{N_q} q_n P_{nq}, \tag{5}$$

$$\langle\hat{p}_c\rangle = \sum_n^{N_p} p_n P_{np}$$

with P_{nq} being the probability of finding a q value in the nth domain and P_{np} being the probability of finding a p value in the nth domain.

Our mode operators are now of the form

$$\hat{a} = 1/2(\hat{q}_c + \delta\hat{q} + i(\hat{p}_c + \delta\hat{p})), \tag{6}$$

The noise properties of the input states can be measured directly by subtracting the closest expected displacement, evaluating the variance of the quantum fluctuations around this expected value, and taking the weighted average over all expected values. These quantities can then be related to $\delta\hat{q}$ and $\delta\hat{p}$ in the following way. We can write the average position quadrature variance described above as

$$
\begin{aligned}
V_q &\equiv \sum_{n}^{N_q}(\langle\hat{q}^2\rangle_n - q_n^2)P_{nq} \\
&= \langle\hat{q}^2\rangle - \sum_{n}^{N_q}q_n^2 P_{nq} \\
&= \langle\hat{q}^2\rangle - \sum_{n}^{N_q}(2\langle\hat{q}\hat{q}_c\rangle_n - \langle\hat{q}_c^2\rangle_n)P_{nq} \\
&= \langle(\hat{q}-\hat{q}_c)^2\rangle \\
&= \langle\delta\hat{q}^2\rangle.
\end{aligned}
\tag{7}
$$

This can be evaluated via

$$
V_q = \int dq\, q^2|\Psi(q)|^2 - \sum_{n}^{N}\frac{(\int_n dq\, q|\Psi(q)|^2)^2}{(\int_n dq|\Psi(q)|^2)},
\tag{8}
$$

where we have used

$$
\begin{aligned}
q_n &= \frac{\int_n dq\, q|\Psi(q)|^2}{\int_n dq|\Psi(q)|^2}; \\
P_{nq} &= \int_n dq|\Psi(q)|^2,
\end{aligned}
\tag{9}
$$

and the integral $\int_n dq$ is taken over the corresponding nth domain, whilst $\Psi(q) = \langle q|\psi\rangle$ is the position wavefunction of the state $|\psi\rangle$. Similarly, the momentum quadrature variance can be written as

$$
\begin{aligned}
V_p &\equiv \langle\delta\hat{p}^2\rangle = \langle(\hat{p}-\hat{p}_c)^2\rangle \\
&= \langle\hat{p}^2\rangle - \langle\hat{p}_c^2\rangle \\
&= \langle\hat{p}^2\rangle - \sum_{n}^{N_p}p_n^2 P_{np}.
\end{aligned}
\tag{10}
$$

This can be evaluated via

$$
V_p = \int dq\, p^2|\Psi(p)|^2 - \sum_{n}\frac{(\int_n dp\, p|\Psi(p)|^2)^2}{(\int_n dp|\Psi(p)|^2)}.
\tag{11}
$$

where the integral $\int_n dp$ is taken over the corresponding nth domain whilst $\Psi(p) = \langle p|\psi\rangle$ is the momentum wavefunction of the state $|\psi\rangle$.

If the signal peaks are localised well in their expected domains, then Equations (8) and (11) will well represent the average spread of the signal peaks. By assuming Gaussian statistics, we can then estimate the probability that a quadrature measurement will find a result in their expected domain via

$$
P_j = Erf\left[\frac{D}{2\sqrt{2V_j}}\right],
\tag{12}
$$

where D is the width of the domains and $j = q, p$.

The interpretation becomes more subtle if the variances approach the width of the domains. If this happens, then the probability distribution within the domain will be "clipped" and changed relative to its "unclipped" value. We will observe this effect in the following examples.

The next two subsections will examine the examples of cat states and GKP states. "Cat state" usually refers to a superposition of differently displaced Gaussian states. The case we consider here is a symmetric superposition of two coherent states around the origin.

The GKP state is a particular superposition of multiple displaced Gaussian states which has the feature that if qubit values of zero or one are encoded by the displacement values in the q quadrature, then the p quadrature encodes the "+" and "−" diagonal states, respectively. This nice feature means that a logical Hadamard gate can be enacted on the encoded states with a simple phase rotation. The specific GKP state construction we use here is a multiple, weighted superposition of squeezed states displaced (and squeezed) in the q direction. Example q quadrature probability distributions for the cat and GKP states are shown in Figures 1–3.

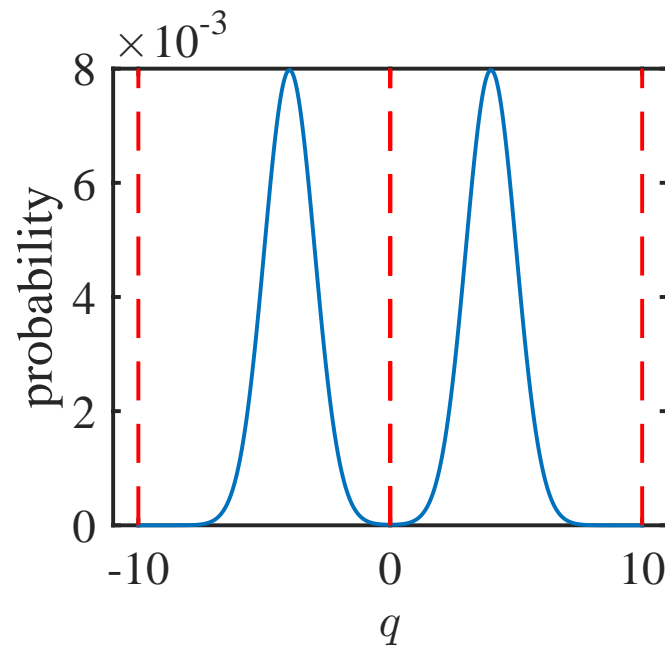**Figure 1.** Example q quadrature probability distribution for the cat state in Equation (13) with $\alpha = 2$.
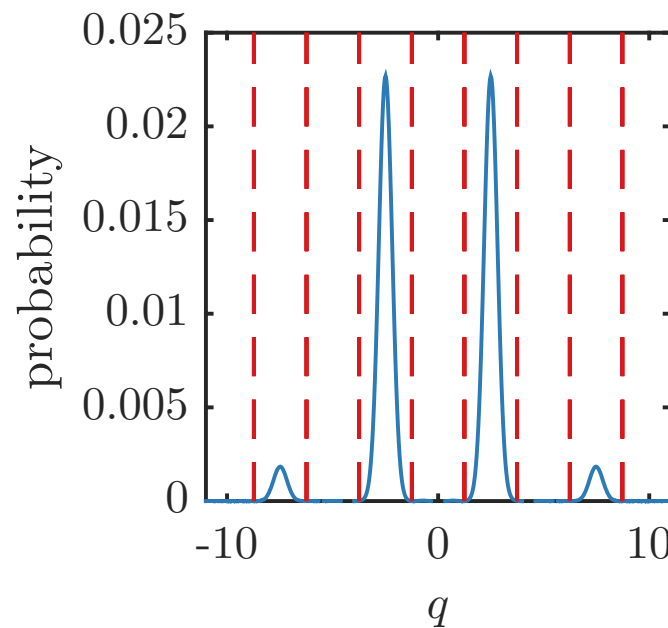

Figure 2. Example q quadrature probability distribution for the GKP state in Equation (20) with $\mu = 1$ and $\Delta^2 = 0.1$.
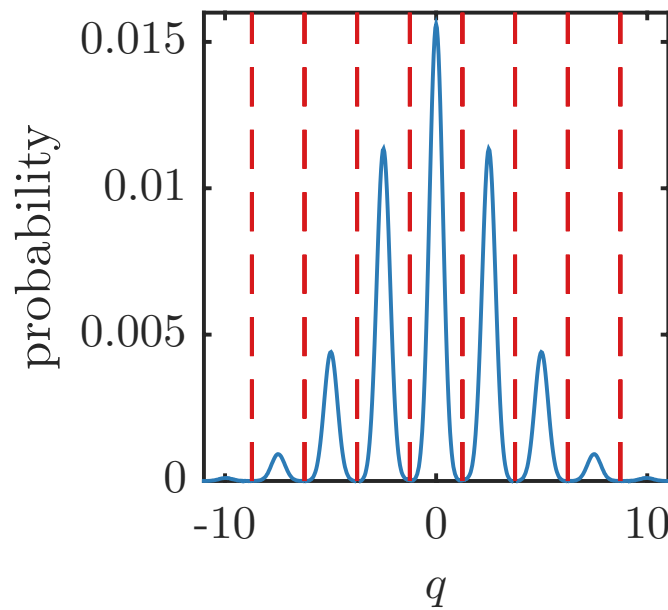
Figure 3. Example q quadrature probability distribution for the GKP state in Equation (20) with $\mu = 1$ and $\Delta^2 = 0.1$ but rotated through a quadrature angle of $\pi/2$. This is equal to the "$-$" GKP state or, equivalently, the p quadrature probability distribution of the "1" state.

2.1. Cat States

Let us us begin with perhaps the simplest non-trivial example: a superposition of two displacements of the vacuum. In particular, let us consider the cat state given by

$$|\psi_c\rangle = \aleph(|\alpha\rangle + |-\alpha\rangle), \tag{13}$$

where $\aleph = (2 + 2e^{-2\alpha^2})^{-1/2}$ is a normalisation constant and $|\pm\alpha\rangle$ are coherent states with real displacements $\pm\alpha$. Consider the position quadrature variance. The wave function is

$$\Psi_q = \aleph(2\pi)^{-1/4}(e^{-(q-2\alpha)^2/4} + e^{-(q+2\alpha)^2/4}). \tag{14}$$

We can take the domain for $n = 1$ as $-\infty \to 0$, and that for $n = 2$ is $0 \to \infty$, leading to the two corresponding values for q_n being

$$q_1 = \frac{\int_{-\infty}^{0} dq \; q|\Psi(q)|^2}{\int_{-\infty}^{0} dq \; |\Psi(q)|^2} \approx -2\alpha \tag{15}$$

$$q_2 = \frac{\int_{0}^{\infty} dq \; q|\Psi(q)|^2}{\int_{0}^{\infty} dq \; |\Psi(q)|^2} \approx 2\alpha,$$

where the approximate equalities are satisfied for $|\alpha| > 1$. The probabilities are given by

$$P_{1q} = \int_{-\infty}^{0} dq \; |\Psi(q)|^2 = 1/2, \tag{16}$$

$$P_{2q} = \int_{0}^{\infty} dq \; |\Psi(q)|^2 = 1/2.$$

By substituting these results into our expressions for V_q, we find that provided $|\alpha| > 1$, then $V_q \approx 1$. This corresponds to our intuitive picture of the cat state comprising two peaks at $\pm\alpha$ with widths of one unit of quantum noise. However, if $|\alpha|$ falls significantly below one, then the distributions in the two domains are only weakly peaked (if at all) and highly

skewed and clipped, and thus the decomposition into a discrete superposition is no longer useful. This is illustrated in Figure 4.
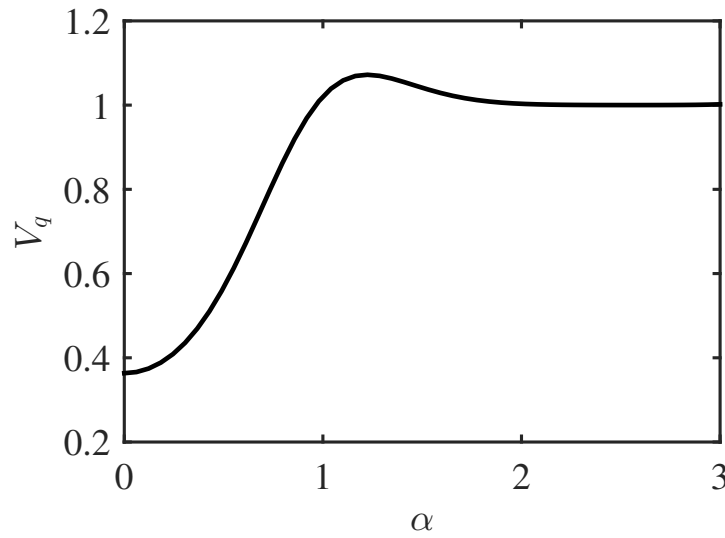

Figure 4. Average position quadrature variance V_q as a function of the parameter α for the cat state defined in Equation (13). Notably, $V_q < 1$ for small values of α, which can be attributed to clipping effects.

Even though the superposition of displacements is only explicit in the position quadrature, interference effects also lead to distinct peaks in the momentum quadrature, around which we can define domains. The momentum wave function is

$$\Psi_p = (1 + e^{-8\alpha^2})^{-1/2}(\pi/2)^{-1/4}e^{-p^2/4}\cos 2p\alpha, \tag{17}$$

and thus we can define the expected value in the nth domain as

$$p_n = \frac{\int_{d_{n,-}}^{d_{n,+}} dp\, p|\Psi(p)|^2}{\int_{d_{n,-}}^{d_{n,+}} dp\, |\Psi(p)|^2} \approx \frac{n\pi}{2\alpha}, \tag{18}$$

with a corresponding probability

$$P_{np} = \int_{d_{n,-}}^{d_{n,+}} dp\, |\Psi(p)|^2 \tag{19}$$

where $d_{n,\pm} = (n \pm 1/2)\pi/(2\alpha)$. When substituting these results into our expressions for V_p, we find that the variances scale inversely with $|\alpha|$. This is unsurprising given that the size of the domains are inversely proportional to $|\alpha|$. In particular, the ratio of the domain size (equivalently peak separation) to the standard deviation ($\frac{n\pi}{2\alpha} / \sqrt{V_p}$) is roughly constant ($\approx 5.7$) for $|\alpha| > 1$.

2.2. GKP States

We now consider the case of GKP states. A physical GKP "zero" state has q quadrature outcome probabilities with peaks around the values $2n\sqrt{2\pi}$, where n is any integer and the peaks are weighted by a suitable envelope function. The corresponding GKP "one" state has q quadrature outcome probabilities peaked around the values $2(n + 1/2)\sqrt{2\pi}$, which are similarly weighted. The p quadrature outcome probabilities for these computational states have peaks at both the "zero" and "one" positions. (i.e., at values $n\sqrt{2\pi}$). This is consistent with the observation that a logical Hadamard gate should be implemented by a $\frac{\pi}{2}$ delay, which takes $\hat{q} \to \hat{p}$ and $\hat{p} \to -\hat{q}$. Thus, the logical values of the p quadrature for

the "zero" and "one" computational basis states correspond to the "+" and "−" dual basis states, respectively.

We will consider a physical example of such a GKP state to see what the noise properties are for such a state. One such example is the squeezed state superpositions [7]

$$|\psi_\mu\rangle = N \sum_{n=-\infty}^{\infty} e^{-\frac{\pi}{2}\Delta^2(2n+\mu)^2}$$
$$\hat{D}\left(\sqrt{\frac{\pi}{2}}(2n+\mu)\sqrt{1-\Delta^4}\right)|\Delta\rangle, \tag{20}$$

where N is a normalisation factor and $|\Delta\rangle$ is a squeezed state with a squeezed variance $\Delta^2 < 1$. The value of μ determines the logical state (i.e., $|\psi_0\rangle$ is the logical "zero" state and $|\psi_1\rangle$ is the logical "one" state). We can evaluate the noise properties of these initial states using Equation (8) and by defining the domains via $(n+1/2)\sqrt{2\pi} < q < (n+3/2)\sqrt{2\pi}$ and similarly for p.

In Figure 5, we plot V_q as a function of Δ^2 for the computational states and the diagonal states. We find that provided $\Delta^2 \lesssim \frac{1}{10}$, then to an excellent approximation

$$V_q = V_p = \Delta^2. \tag{21}$$

This is true for all logical states. This indicates that, provided the squeezing is sufficiently strong, these states behave as hoped with the superposed "spikes" giving the logical value, modulated by Gaussian noise with a variance equal to the squeezing, in both quadratures. Alternatively, given that this is an expected result for GKP states [4], one can take this as indicating that our Heisenberg approach can successfully factor the operators into signal and noise parts in a consistent way for such states. However, at lower levels of squeezing (i.e., larger Δ), state-dependent effects are seen. For the computational states, this mostly occurs due to "clipping" of the distribution by the domain boundary such that the calculated V_q no longer aligns well with the actual variance around the spikes. On the other hand, the deviation of the diagonal states from the expected behaviour is predominantly due to our approximate GKP states no longer exhibiting the expected noise symmetry between the spikes in different quadratures.
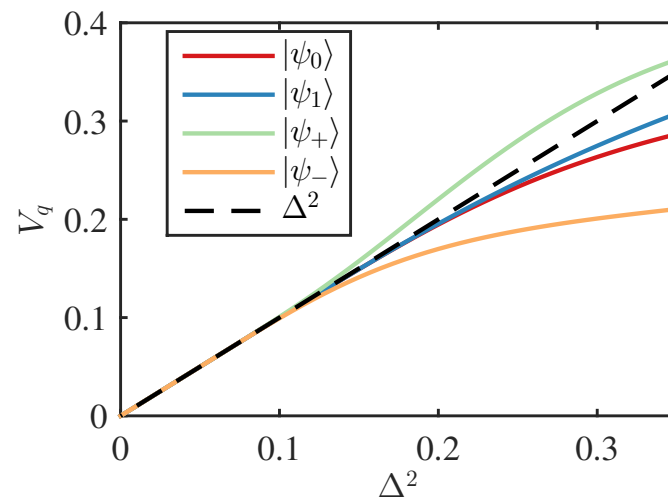

Figure 5. Average position quadrature variance V_q as a function of the squeezing parameter Δ^2 for GKP logical states. The computational-basis states are defined in Equation (20), and the dual-basis states are simply rotated versions of the computational-basis states. The dashed line represents Δ^2. V_q matches Δ^2 for small values of Δ but deviates in a state-dependent way for larger values. Plotting V_p follows a similar approach, as the p quadrature is simply a rotation, with the computational and dual-basis states switching roles.

3. Operator Evolution and Feedforward

Recall that our mode operators can be written in the form of Equation (6). Using operators of this kind to represent the various input modes that interact in an optical circuit, we can proceed to evolve them through beamsplitters, squeezers, and other quadratic unitaries (linear in the mode operators) in the usual way whilst keeping track of their noise and signal properties. For example, suppose our initial mode, Equation (6), passes through a loss such that only the fraction η is transmitted. Our output mode is

$$\hat{a}_l = 1/2(\sqrt{\eta}(\hat{q}_c + \delta\hat{q} + i(\hat{p}_c + \delta\hat{p})) + \sqrt{1-\eta}(\hat{q}_v + i\hat{p}_v)), \tag{22}$$

where $\hat{q}_v$ and $\hat{p}_v$ are the position and momentum quadrature operators of the vacuum mode introduced by the loss, respectively. By inspection, we see that the expected signal values (and hence corresponding domain boundaries) have been scaled by the factor $\sqrt{\eta}$. On the other hand, the variances around these expected values are now

$$
\begin{aligned}
V_{ql} &= \eta\langle\delta\hat{q}^2\rangle + (1-\eta)\langle\delta\hat{q}_v^2\rangle \\
&= \eta V_q + (1-\eta),
\end{aligned}
\tag{23}
$$

and

$$
\begin{aligned}
V_{pl} &= \eta\langle\delta\hat{p}^2\rangle + (1-\eta)\langle\delta\hat{p}_v^2\rangle \\
&= \eta V_p + (1-\eta),
\end{aligned}
\tag{24}
$$

where we make use of the vacuum noise being independent and having unit variance. Considering our cat state example from the previous section, we see that there is no effect on the position quadrature variance, as we still have $V_{ql} = 1$. The detrimental effect of loss on position only arises from the scaling down of the expected values closer to the domain boundary at zero. On the other hand, given that for $|\alpha| > 1$, $V_p << 1$, the effect on the momentum quadrature is a significant broadening of the peaks for relatively small amounts of loss. This, combined with the reduction in peak separation, rapidly washes out the interference fringes entirely, especially for $|\alpha| >> 1$. This illustrates the well-known fragility of cat states in the face of a loss.

As well as optical unitary evolution, many quantum circuits involve quadrature measurements followed by a feedforward to other modes in the circuit. In particular, this can occur in teleportation scenarios arising in error correction [10], cluster state [11] protocols, or both [5]. A feedforward of quadrature measurements can be represented in the usual way [1] by feeding forward some function of the measurement operator. Thus, a typical output mode $\hat{a}_o$ after a teleportation-type circuit might be written formally as

$$\hat{a}_o = 1/2(\hat{q}_{co} + \delta\hat{q}_o + i(\hat{p}_{co} + \delta\hat{p}_o)) + G_1(\hat{q}_1) + iG_2(\hat{p}_2), \tag{25}$$

where a feedforward from an earlier position measurement ($\hat{q}_1$) and another from an earlier momentum measurement ($\hat{p}_2$), have been incorporated. In standard teleportation, the "G" functions would be linear functions of the measurement operators (i.e., $G_1(\hat{q}_1) = g_1\hat{q}_1$ and $G_2(\hat{p}_2) = g_2\hat{p}_2$). However, in a situation where we can usefully write our measurement operators as $\hat{q}_1 = \hat{q}_{c1} + \delta\hat{q}_1$ and $\hat{p}_2 = \hat{p}_{c2} + \delta\hat{p}_2$, we can perform error correction by shifting to the nearest "ideal" result in each domain, represented by $\hat{q}_{c1}$ or $\hat{p}_{c2}$. Hence, we now have the highly nonlinear feedforward functions $G_1(\hat{q}_1) = g_1\hat{q}_{c1}$ and $G_2(\hat{p}_2) = g_2\hat{p}_{c2}$, and our output mode is now written formally as

$$\hat{a}_o = 1/2(\hat{q}_{co} + \delta\hat{q}_o + i(\hat{p}_{co} + \delta\hat{p}_o)) + g_1\hat{q}_{c1} + ig_2\hat{p}_{c2}. \tag{26}$$

To illustrate a feedforward with error correction, we will consider a simple GKP circuit.

4. GKP Error Correction

Another useful feature of GKP states is that small displacements of the state, as will naturally arise in the presence of loss or thermal noise, can be corrected by a straightforward circuit. This process is often referred to as GKP error correction. In the following, we will analyse such a GKP error correction circuit.

The circuit we will consider is shown in Figure 6. It is an example of a continuous-variable teleportation circuit with error correction, where we assume both resource states are approximate GKP states and we neglect loss. We will label the approximate GKP input and two resource states with the subscripts "$1, 2, 3$", respectively. The resource states in modes "2" and "3" are prepared in the logical "$+$" state, whilst the input in mode "1" is in an arbitrary GKP logical state.
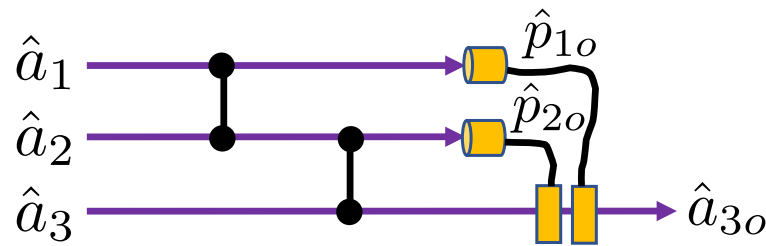

Figure 6. Simple teleportation circuit with CZ gates to interact with the modes and feedforward of momentum measurements of mode 1 as imaginary displacements of mode 3 and momentum measurements of mode 2 as real displacements of mode 3. The measurement of mode 1 is represented by the operator $\hat{p}_{1o}$, but if error correction is being implemented, then it is $\hat{p}_{c1o}$, which is fed forward. Similarly, the measurement of mode 2 is represented by the operator $\hat{p}_{2o}$, but if error correction is being implemented, then it is $\hat{p}_{c2o}$, which is fed forward.

4.1. Ideal Case

The action of a continuous variable CZ gate is to displace the value of the $\hat{p}$ quadrature of one mode by the value of the $\hat{q}$ quadrature of the other mode whilst leaving the $\hat{q}$ quadratures unchanged [11]. Hence, for the circuit in Figure 6, the $\hat{p}$ quadratures will evolve such that $\hat{p}_1 \to \hat{p}_1 + \hat{q}_2$, $\hat{p}_2 \to \hat{p}_2 + \hat{q}_1 + \hat{q}_3$ and $\hat{p}_3 \to \hat{p}_3 + \hat{q}_2$. Using these expressions and the error correction feedforward relations previously introduced, we can write the expression for the output mode as follows:

$$
\begin{aligned}
\hat{a}_{3o} \;=\; & \frac{1}{2}(\hat{q}_{c3} + \delta\hat{q}_3 + i(\hat{p}_{c3} + \delta\hat{p}_3)) + \\
& \frac{i}{2}(\hat{q}_{c2} + \delta\hat{q}_2) - \frac{i}{2}p_{c1o} - \frac{1}{2}p_{c2o},
\end{aligned}
\tag{27}
$$

where we have

$$
\begin{aligned}
\hat{p}_{1o} \;&=\; \hat{p}_{c1} + \delta\hat{p}_1 + \hat{q}_{c2} + \delta\hat{q}_2, \\
\hat{p}_{2o} \;&=\; \hat{p}_{c2} + \delta\hat{p}_2 + \hat{q}_{c1} + \delta\hat{q}_1 + \hat{q}_{c3} + \delta\hat{q}_3,
\end{aligned}
\tag{28}
$$

and therefore

$$
\begin{aligned}
G(\hat{p}_{1o}) \;&=\; \hat{p}_{c1o}, \\
G(\hat{p}_{2o}) \;&=\; \hat{p}_{c2o}.
\end{aligned}
\tag{29}
$$

If we assume that the noise terms are sufficiently small that it is unlikely that the noise causes measured values to leave their nominal domains, then we can approximate the feedforward terms as follows:

$$\begin{aligned}\hat{p}_{c1o} &\approx \hat{p}_{c1} + \hat{q}_{c2},\\ \hat{p}_{c2o} &\approx \hat{p}_{c2} + \hat{q}_{c1} + \hat{q}_{c3}.\end{aligned}\tag{30}$$

and hence

$$\hat{a}_{3o} = \frac{1}{2}(\delta\hat{q}_3 + i\delta\hat{p}_3 + i\delta\hat{q}_2 + \hat{p}_{c2}) - \frac{1}{2}(\hat{q}_{c1} + i\hat{p}_{c1}).\tag{31}$$

The logical state of the output matches that of the input as seen from the output signal terms $\hat{q}_{c1} + i\hat{p}_{c1}$. Notice that because the resource states are prepared in the "+" state, the term in the output signal $\hat{p}_{c2}$ has a known logical "zero" value, and thus its addition to the output does not change the overall logical value. Three noise terms are also added to the output.

The circuit can be iterated by taking $\hat{a}_{3o}$ as mode 1 of the next circuit and introducing new resource states at mode 2 and mode 3. The output mode and variances separate conveniently into deterministic displacement terms and noise terms (the "δ" terms). The error correction feature of the circuit can be seen from the fact that none of the noise terms in the output depend on the input; that is, even though there is still noise in the output, the noise does not "build up" as we iterate but rather is "refreshed" from new resource states used at each round.

4.2. Loss Tolerance

We now consider the situation depicted in Figure 7, in which loss affects the input state, the resource states, and all of the elements in the error correction circuit. We use our Heisenberg approach to demonstrate that the error correction properties of the circuit are loss-tolerant, provided we add an additional loss element and a linear amplifier in appropriate positions on the third rail.
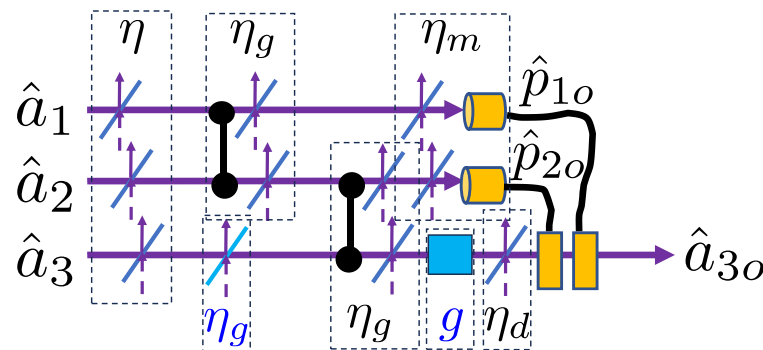

Figure 7. The simple teleportation error correction circuit of Figure 3 but with loss errors included for all components. The loss is modelled with beamsplitters, where the transmission of the beamsplitters represents the efficiency of the corresponding components. Additional components (loss and linear amplification of mode 3) are indicated in blue. These components, along with tailored feedforward gains, allow the circuit to still implement error correction. The measurement of mode 1 is represented by the operator $\hat{p}_{1o}$, but if error correction is being implemented, then it is $\hat{p}_{c1o}$ which is fed forward. Similarly, the measurement of mode 2 is represented by the operator $\hat{p}_{2o}$, but if error correction is being implemented, then it is $\hat{p}_{c2o}$ which is fed forward.

As shown in Figure 7, loss was added to the input and resource states. For simplicity, we used the same beamsplitter transmission value, η, for all of the modes. We modelled the loss in the CZ gates by placing beamsplitters with transmission η_g after each gate. Similarly, we modelled detection inefficiency by placing beamsplitters with transmission η_m before the detectors and loss in the displacement operations by placing a beamsplitter of transmission η_d before the displacements. In order to balance the loss, the experimenter

should purposely add an additional beamsplitter with transmission η_g to the third mode before the CZ gate. Finally, to ensure the output is balanced and centred in the domains, a linear amplifier of gain g was applied to the third rail after the CZ gate.

To see how this works, we first write the evolved operators describing the outcomes at the first and second momentum measurements as

$$
\hat{p}_{1o} = \sqrt{\eta}\sqrt{\eta_g}\sqrt{\eta_m}\left(\hat{p}_{c1} + \delta\hat{p}_1 + \hat{q}_{c2} + \delta\hat{q}_2\right)
$$
$$
+ \sqrt{\eta_m}\sqrt{1 - \eta_g\eta}\,(\delta\hat{q}_{v2} + \delta\hat{p}_{v1}) + \sqrt{1 - \eta_m}\delta\hat{p}_{m1} \tag{32}
$$

$$
\hat{p}_{2o} = \eta_g\sqrt{\eta}\sqrt{\eta_m}\left(\hat{p}_{c2} + \delta\hat{p}_2 + \hat{q}_{c1} + \delta\hat{q}_1 + \hat{q}_{c3} + \delta\hat{q}_3\right)
$$
$$
+ \sqrt{\eta_m}\sqrt{1 - \eta_g^2\eta}\,(\delta\hat{q}_{v1} + \delta\hat{q}_{v3} + \delta\hat{p}_{v2})
$$
$$
+ \sqrt{1 - \eta_m}\delta\hat{p}_{m2}. \tag{33}
$$

Here, $\delta\hat{p}_{vi}$ and $\delta\hat{q}_{vi}$ are vacuum operators for the momenta and position, respectively, arising from the input mode and gate loss, while $\delta\hat{p}_{mi}$ represents the vacuum operators for the momenta arising from detector inefficiency.

Consider the first momentum measurement. Using the error correction strategy and a feedforward gain of $g_1 = -\frac{1}{\sqrt{\eta\eta_g\eta_m}}$, we find the feedforward operators to be approximately

$$
\hat{p}_{c1o} \approx \hat{p}_{c1} + \hat{q}_{c2} \tag{34}
$$

This assumes that the variance of the feedforward operators

$$
V_1 = 2\Delta^2 + 2\left(\frac{1}{\eta\eta_g} - 1\right) + \frac{1}{\eta\eta_g}\left(\frac{1}{\eta_m} - 1\right), \tag{35}
$$

is sufficiently small.

Now, we consider the second momentum measurement. Using the error correction strategy and a feedforward gain of $g_2 = -\frac{1}{\sqrt{\eta\eta_g^2\eta_m}}$, we find the feedforward operators to be approximately

$$
\hat{p}_{c2o} \approx \left(\hat{p}_{c2} + \hat{q}_{c1} + \hat{q}_{c3}\right). \tag{36}
$$

This now assumes that the variance of the feedforward operators

$$
V_2 = 3\Delta^2 + 3\left(\frac{1}{\eta\eta_g^2} - 1\right) + \frac{1}{\eta\eta_g^2}\left(\frac{1}{\eta_m} - 1\right), \tag{37}
$$

is sufficiently small.

Finally, we can consider the third mode. Its momentum operator directly after the CZ gate is given by

$$
\hat{p}'_3 = \sqrt{\eta}\sqrt{\eta_g^2}\left(\hat{p}_{c3} + \delta\hat{p}_3 + \hat{q}_{c2} + \delta\hat{q}_2\right)
$$
$$
+ \sqrt{1 - \eta_g^2\eta}\,(\delta\hat{q}_{v2} + \delta\hat{p}_{v3}). \tag{38}
$$

After linear amplification with $g = \frac{1}{\sqrt{\eta\eta_g^2\eta_d}}$, passing through the displacement loss, and the subsequent displacement by $\hat{p}_{c1o}$ and $\hat{p}_{c2o}$, the output momentum operator of the third mode is given by

$$\hat{p}_3'' = -\hat{p}_{c1} + \hat{p}_{c3} + \delta\hat{p}_3 + \delta\hat{q}_2$$

$$+ \sqrt{\frac{1}{\eta_g^2\eta} - 1}\,(\delta\hat{q}_{v2} + \delta\hat{p}_{v3})$$

$$- \sqrt{\eta_d}\sqrt{\frac{1}{\eta_g^2\eta\eta_d} - 1}\,\delta\hat{p}_{v4} + \sqrt{1 - \eta_d}\,\delta\hat{p}_d. \tag{39}$$

Similarly, we can write the final position operator for the third mode as follows:

$$\hat{q}_3'' = -\hat{q}_{c1} - \hat{p}_{c2} + \delta\hat{q}_3$$

$$+ \sqrt{\frac{1}{\eta_g^2\eta} - 1}\,\delta\hat{q}_{v3}$$

$$- \sqrt{\eta_d}\sqrt{\frac{1}{\eta_g^2\eta\eta_d} - 1}\,\delta\hat{q}_{v4} + \sqrt{1 - \eta_d}\,\delta\hat{q}_d, \tag{40}$$

and hence we can write

$$\hat{a}_{3o} = \frac{1}{2}(\hat{q}_3'' + i\hat{p}_3''). \tag{41}$$

Although additional noise is added compared with Equation (31), the error correction feature of the circuit can still be seen from the fact that none of the noise terms in the output depend on the input. Again, even though there is still noise in the output, the noise does not "build up" as we iterate but rather is "refreshed" from new resource states at each round. Of course, the extra noise introduced will need to be small and may require stronger squeezing of the source states.

4.3. Logical Errors

Thus far, we have assumed that the measurement and feedforward always correct to the right ideal solution, such as in Equation (30). However, as we saw from Equation (12), even if the peaks are localised well, there is a nonzero probability $1 - P_j$ that they will fall outside their nominal domain. If this happens, then the wrong displacement will be fed forward. For example, for GKP states, if we wrongly identify a q measurement falling on the right side of a peak with the neighbouring domain, then the ideal "spikes" will be shifted by $\sqrt{2\pi}$. Similarly, if we wrongly identify a q measurement falling on the left side of a peak with the neighbouring domain, then the ideal "spikes" will be shifted by $-\sqrt{2\pi}$. After being fed forward, this will lead to bit flip or phase flip errors in the output state.

Given this, a better approximation for the feedforward operators is

$$\begin{aligned}
\hat{p}_{c1o} &= \hat{p}_{c1} + \hat{q}_{c2} + \hat{p}_{e1}, \\
\hat{p}_{c2o} &= \hat{p}_{c2} + \hat{q}_{c1} + \hat{q}_{c3} + \hat{p}_{e2},
\end{aligned} \tag{42}$$

where $\hat{p}_{ei}$ represents error operators with discrete outcomes $n\sqrt{2\pi}$. If $n = 0$, then there is no error. This occurs with a probability $P_i^{(0)} = Erf[\frac{D}{2\sqrt{2V_i}}]$. Errors happen when $n \neq 0$, and these occur with probabilities $P_i^{(n)} = (Erf[\frac{(|n|+1)D}{2\sqrt{2V_i}}] - Erf[\frac{|n|D}{2\sqrt{2V_i}}])$. The variances V_i are the total noises on the detected quadratures. For example, in the ideal case, from Equation (28)

we have $V_1 = \langle \delta \hat{q}_2^2 \rangle + \langle \delta \hat{p}_1^2 \rangle$ and $V_2 = \langle \delta \hat{q}_1^2 \rangle + \langle \delta \hat{q}_3^2 \rangle + \langle \delta \hat{p}_2^2 \rangle$. The output operator can then be written more accurately as

$$
\begin{aligned}
\hat{a}_{3o} &= \frac{1}{2} (\delta \hat{q}_3 + i \delta \hat{p}_3 + i \delta \hat{q}_2 + \hat{p}_{c2}) \\
&\quad - \frac{1}{2} (\hat{q}_{c1} + \hat{p}_{e2} + i \hat{p}_{c1} + i \hat{p}_{e1}).
\end{aligned}
\tag{43}
$$

Notice that these mistakes do not change the noise properties, but now we can also track the signal errors as the system is iterated. A logical error encoding and correction scheme is required in order to correct the signal errors [10]. We believe that such multi-mode codes could also be tractable to analyse using our approach. However, the complexity of the error tracking required may become more challenging.

5. Discussion and Conclusions

In this paper, we presented signal and noise analysis of both cat states and GKP states to highlight the generality of our approach. In particular, the analysis of the preceeding section demonstrates the power and relative simplicity of this approach while also highlighting the necessity for the total noise variances to be small. Given that we are grouping noise from several sources together and associating it with arbitrary logical states, it is important that we are in a regime where the noise affects different states in the same way. Figure 5 shows that this is true for GKP states, provided the squeezing is 10 dB or higher, as was observed previously. Whilst this may seem a bit restrictive, it should be remembered that for large quantum circuits to perform faithfully, they inevitably need to operate in this high-fidelity regime anyway [5,12]. This also applies to quantum communication applications [13]. Hence, we expect our approach to prove useful in tracking the flow of noise, signals, and errors in quantum computing circuits employing GKP and other Bosonic qubits. Finally, we demonstrated the power these techniques can have to develop new schemes with a loss-tolerant generalisation of the simple teleportation circuit considered, allowing for general loss rates for each component.

References

1. Bachor, H.; Ralph, T.C. *A Guide to Experiment in Quantum Optics*, 3rd ed.; Wiley: Hoboken, NJ, USA, 2019.
2. Weedbrook, C.; Pirandola, S.; García-Patron, R.; Cerf, N.J.; Ralph, T.C.; Shapiro, J.H.; Lloyd, S. Gaussian Quantum Information. *Rev. Mod. Phys.* **2012**, *84*, 621. [CrossRef]
3. Ralph, T.C.; Gilchrist, A.; Milburn, G.J.; Munro, W.J.; Glancy, S. Quantum Computation with Coherent Optical States. *Phys. Rev. A* **2003**, *68*, 042319. [CrossRef]
4. Gottesman, D.; Kitaev, A.; Preskil, J. Encoding a qubit in an oscillator. *Phys. Rev. A* **2001**, *64*, 012310. [CrossRef]
5. Menicucci, N.C. Fault-Tolerant Measurement-Based Quantum Computing with Continuous-Variable Cluster States. *Phys. Rev. Lett.* **2014**, *112*, 120504. [CrossRef] [PubMed]
6. Pantaleoni, G.; Baragiola, B.Q.; Menicucci, N.C. Modular bosonic subsystem codes. *Phys. Rev. Lett.* **2020**, *125*, 040501. [CrossRef] [PubMed]
7. Tzitrin, I.; Bourassa, J.E.; Menicucci, N.C.; Sabapathy, K.K. Progress towards practical qubit computation using approximate Gottesman-Kitaev-Preskill codes. *Phys. Rev. A* **2020**, *101*, 032315. [CrossRef]

8.   Bourassa, J.E.; Alexander, R.N.; Vasmer, M.; Patil, A.; Tzitrin, I.; Matsuura, T.; Su, D.; Baragiola, B.Q.; Guha, S.; Dauphinais, G.; et al. Blueprint for a scalable photonic fault-tolerant quantum computer. *Quantum* **2021**, *5*, 392. [CrossRef]

9.   Hillmann, T.; Quijandría, F.; Grimsmo, A.L.; Ferrini, G. Performance of Teleportation-Based Error-Correction Circuits for Bosonic Codes with Noisy Measurements. *PRX Quantum* **2022**, *3*, 020334. [CrossRef]

10.   Glancy, S.; Knill, E. Error analysis for encoding a qubit in an oscillator. *Phys. Rev. A* **2006**, *73*, 012325. [CrossRef]

11.   Menicucci, N.C.; van Loock, P.; Gu, M.; Weedbrook, C.; Ralph, T.C.; Nielsen, M.A. Universal Quantum Computation with Continuous-Variable Cluster States. *Phys. Rev. Lett.* **2006**, *97*, 110501. [CrossRef] [PubMed]

12.   Baragiola, B.Q.; Pantaleoni, G.; Alexander, R.N.; Karanjai, A.; Menicucci, N.C. All-Gaussian Universality and Fault Tolerance with the Gottesman-Kitaev-Preskill Code. *Phys. Rev. Lett.* **2019**, *123*, 200502. [CrossRef] [PubMed]

13.   Schmidt, F.; Miller, D.; van Loock, P. Error-corrected quantum repeaters with Gottesman-Kitaev-Preskill qudits. *Phys. Rev. A* **2024**, *109*, 042427. [CrossRef]